JOURNAL OF RESEARCH of the National Bureau of Standards—D. Radio Propagation
Vol. 65D, No. 3, May–June 1961

Diversity Effects in Long Distance High Frequency Radio Pulse Propagation[1, 2]

S. A. Bowhill [3]

(August 15, 1960; revised January 4, 1961)

Spaced antenna measurements are described, made on a 8,600-km path between Colombo, Ceylon, and Great Baddow, England, using pulsed radio signals. Simple interpretations in terms of E and F region multiple reflections give good agreement with observed delays for the various echoes.

The correlation between echo amplitudes at spaced antennas was found to be much greater for a pulsed signal than for a CW signal, indicating that most of the diversity in long-distance CW transmission arises through phase incoherence between the various orders of reflection.

1. Introduction

A study of the ionospheric irregularities responsible for the fading of long distance radio signals can best be accomplished by oblique incidence pulse measurements. Previous workers [Wilkins and Kift, 1957: Silberstein, 1958] have shown that very complex modes of propagation may be present on long-distance paths. Detailed theoretical study of these modes has been lacking until recently, when Kift (1960) gave a very detailed method for studying the entire propagation path.

This paper describes the basic phenomena involved, and gives some experimental results obtained on 16.16 Mc/s frequency, using transmissions from Colombo, Ceylon, received at Great Baddow, England.

The complicated pattern of the pulse signal received led to a consideration of possible reflection mechanisms; third and other order F region reflections were found, with E region multiples present on occasion. The complexity of a typical pattern implies that it is a difficult matter to distinguish, in the CW case, between fading due to phase interference between different orders of reflection, and fading of the reflections themselves.

The path differences for the various modes are calculated in section 2, and the experiments are described in section 3. Section 4 compares the calculated path differences with those experimentally observed; the fading analysis is given in section 5.

[1] The work described in this paper was performed by the author while at Marconi's Wireless Telegraph Co., Ltd., Baddow Research Laboratories, Great Baddow, Essex, England.

[2] Paper presented at the Conference on Transmission Problems Related to High-Frequency Direction Finding, at UCLA, June 21–24, 1960.

[3] Ionosphere Research Laboratory, Pennsylvania State University, University Park, Pa.

2. Ray Theory of Long-Distance Propagation

A radio wave traveling a long distance between points on the earth's surface, such as A and M (fig. 1), may be reflected sometimes by the E layer and sometimes by the F layer. In section 2.1, the elementary theory (ignoring ionospheric tilts) for a thin layer is given; in section 2.2, this is extended to include a sporadically occurring layer at a lower height than the main reflection. Section 2.3 describes how a layer of finite thickness may be quickly allowed for.

2.1. Single Thin Layer

For any particular path, the distance d of the receiver from the transmitter is fixed, and the only variables needed to determine all the properties of a particular mode of propagation are the height of the reflecting layer, h, and the order n of the reflection, i.e., the number of "hops" the radio wave makes from the earth to the layer and back over its path. If the angle of arrival, the angle the wave makes

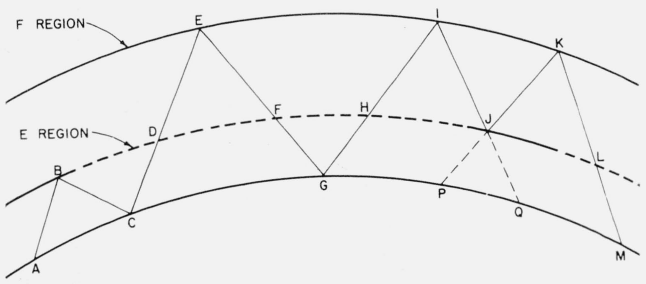

FIGURE 1. *Typical reflection geometry.*

with the horizontal at the earth's surface, is θ, one may write the relations

$$d=R\sin(d/2nR)\tan(\theta+d/2nR)-R+R\cos(d/2nR), \tag{1}$$

$$p=2nR\sin(d/2nR)\sec(\theta+d/2nR)-d, \tag{2}$$

where p=path difference between the reflected wave and a wave traveling directly over the earth's surface.

The eqs (1) and (2) may be regarded as a parametric equation for p in terms of h.

Numerical application of the formulas gives the set of curves shown in figure 2. Three sets of curves are shown on this graph. The first set, for integral values of n, the order of reflection, shows the variation of the time delay p with the height of the reflecting layer, and it is evident that the greater the height of reflection, the greater will be the spacing between successive orders of reflection in the pulse pattern.

Not all the orders of reflection shown are possible in any practical case. Firstly, if we neglect diffraction effects, it is not possible for radio waves to arrive at the receiver with effective angles of arrival less than zero. A set of curves has therefore been drawn showing the angles of arrival of the different orders of reflection at various layer heights. These curves of constant angle of arrival happen to be nearly straight lines, and also are approximately parallel. This implies a relation between the relative time delay of an order of reflection and its angle of arrival, practically independent of the height of reflection. The upper limit is determined by the electron concentration of the ionized layer. The greater this concentration, the steeper the angle at which a radio wave may be incident upon it and still be reflected. This is expressed by the relationship,

$$f=f_0 \sec i,$$

where f=radio wave frequency,
i=angle of incidence of wave at layer=$(n/2)-\theta-d/2nR$,
f_0=vertical incidence critical frequency of the layer.

As the graph is constructed for a particular frequency, namely 16.16 Mc/s, curves of constant f can be drawn in on figure 2. If the vertical incidence critical frequency of the layer is known, the highest permissible order or reflection may be directly read off.

It is now necessary to compare these theoretical suggestions with actual ionospheric data observed at vertical incidence pulse sounders for the period in question. The path from Colombo to Great Baddow passes, in the main, over a region where there are no pulse sounders whose results are regularly available. However, use may be made of the control-point method, which is normally applied to predicting the behavior of long-distance HF propagation paths.

The western control point is fairly near the ionosphere station at Graz, Austria, while the eastern point is at the same latitude as Bombay, and not too far removed in longitude. Mean ionospheric data for the month of July, 1953 are available from these two ionospheric sounding stations, and are given in table 1, with allowance for the difference between G.m.t. and the local solar time at the control

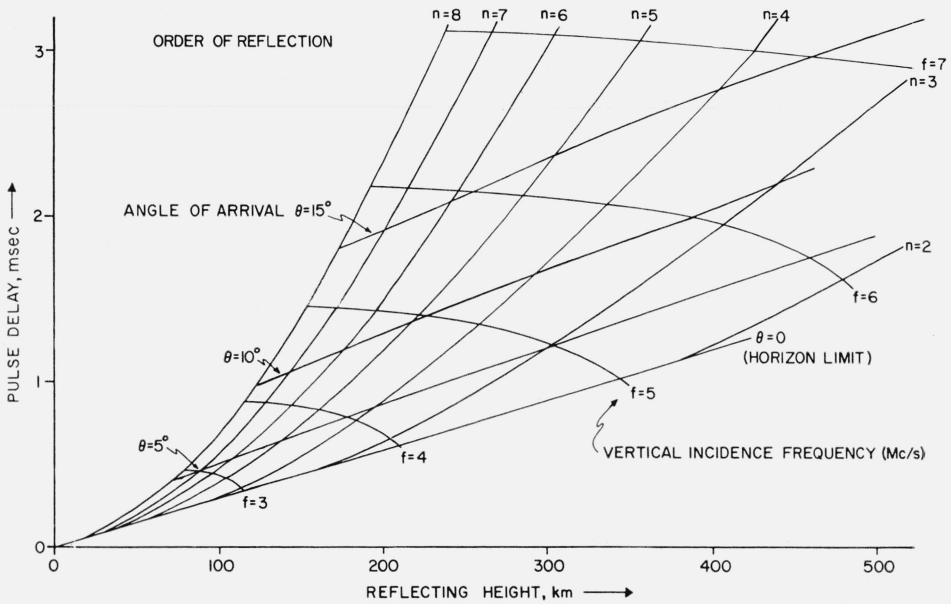

FIGURE 2. *Colombo-Baddow path delays.*

TABLE 1

Time G.m.t.	E. control point		W. control point		Mean virtual height
	$f^\circ F2$	$h' F2$	$f^\circ F2$	$h' F2$	
	Mc/s	*km*	*Mc/s*	*km*	*km*
08	9.0	433	4.9	300	366
09	9.3	432	5.0	315	374
10	9.6	419	5.2	300	360
11	9.5	408	5.2	340	374
12	9.3	383	5.1	310	346
13	8.8	361	5.0	330	346
14	8.1	327	5.0	320	324
15	7.0	324	4.9	300	312
16	5.9	316	5.0	310	313
17	4.8	311	5.0	280	296

point. It is clear that the ionization density at the western control point is the limiting factor, except at 1700 G.m.t.

Corresponding values of the effective reflection height and limiting frequency for the western control point have been plotted in figure 3 for each hour in the afternoon. If a line is drawn vertically downwards from the point corresponding to any hour, it should intersect the curves of constant n at the experimentally observed values of delay. This will be compared with experimental data in section 4.

2.2. Multiple Thin Layers

In this section a simple graphical method will be described for deriving the theoretically expected pulse pattern if multiple reflections are present. It will be assumed that the signal is propagated by reflection at two sharply bounded layers, situated at known heights. The upper layer *EIK* on figure 1, will be assumed uniform in properties, while the lower layer *DFHJL* will be taken to be inhomogeneous in the horizontal direction. At B and J it is present, and reflects the ray; at D, F, H, and L it is absent, and the ray passes through the layer without deviation. The reflection at B is an "E" reflection; that at E is an "F" reflection; while that at I, J, and K will be termed an "M" reflection.

Two points must be noted about this type of propagation. The first is that, provided the numbers of each type of reflection remain the same, they may be permuted in any order without affecting the characteristics of the received signal. The second is that the angle of departure of signal at A is equal to the angles of arrival at C, G, and M, and also determines directly the angles of incidence of the ray at the two layers, since they are at predetermined heights.

The characteristics of the M mode of propagation are closely related to the E and F reflections. In fact, as can be seen from figure 1, if the extension lines JP and JQ are drawn, its transmission distance $GPQM$ is equal to that of two F reflections, less that of one E reflection. The total transmission distance $GHIJKLM$ is also equal to that of a $2F$ reflection less that of a $1E$ reflection. So M reflections will not be treated separately, but simply included as $2F+\bar{1}E$ reflections, where $\bar{1}$ denotes a negative order of reflection. For instance, the path illustrated in figure 1 is just equivalent to $1E+1F+2F-1E=3F$.

If propagated solely by reflection at the E layer or the F layer, let a ray make N_E or N_F hops, respectively, in traveling a distance d (the fact that N_E and N_F may be fractional presents no analytical difficulty; they may be regarded as obtained by interpolation between integral values of N_E and N_F for the particular value of θ). The ray therefore travels a distance d/N_E in one E hop, and d/N_F in one F hop. If the ray makes mE reflections and nF

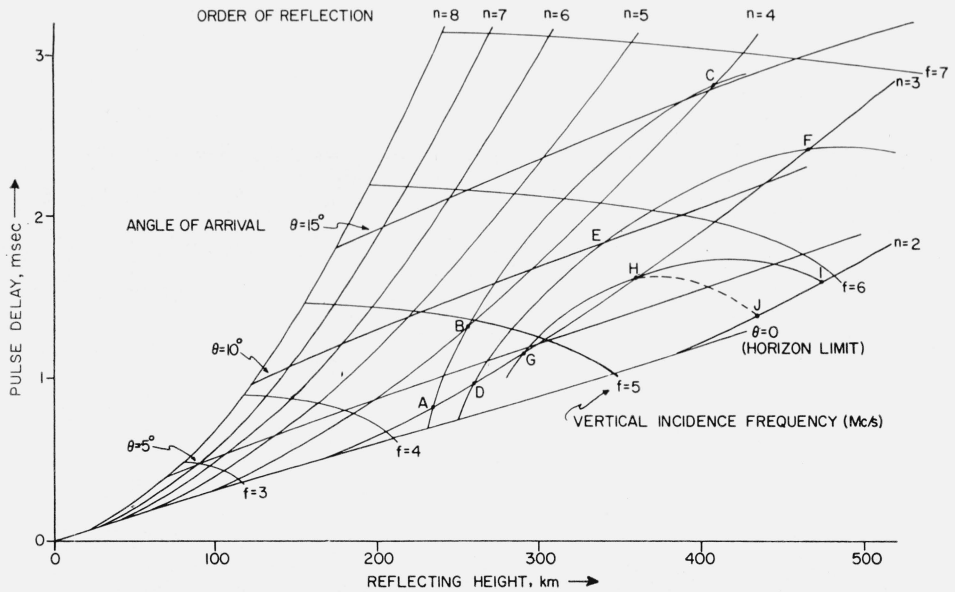

FIGURE 3. *Thick layer delays for July 3, 1953.*

reflections, clearly

$$\frac{m}{N_E}+\frac{n}{N_F}=1. \tag{3}$$

It is convenient to represent the various orders of reflection on a graph like figure 4. Each intersection of integral ordinates and abscissas represents a possible mode of propagation. Points along the horizontal axis represent rays propagating by 1, 2, 3, etc., reflections at the E layer alone; similarly, on the vertical axis they represent reflections occurring at the F layer alone. Points not lying on either axis represent mixed modes of propagation, partly E and partly F.

Now eq (3) is just the equation of a straight line on this diagram, since N_E and N_F are constant for constant θ. The full lines on figure 4 are for $\theta=0°$, 5°, 10°, 15°, and 20°, for a height of reflection of 120 km for the E layer, and 250 km for the F layer.

The points on the negative side of the E axis represent the M type reflections mentioned previously; for instance, the point P on figure 4 is $6F+\bar{3}E$, or 3 M reflections. A line has been drawn from the origin with a slope of -1; no intersections on or below this have any physical meaning.

One may easily find the total time delay of a mixed order of reflection. If the ray would be delayed by p_E or p_F when propagated entirely by reflection at the E or F regions respectively, then its delay for unit distance is p_E/d and p_F/d; the delay experienced by an mE nF echo is then

$$p=p_E\cdot\frac{m}{N_E}+p_F\cdot\frac{n}{N_F}. \tag{4}$$

The loci of constant p on figure 4 are therefore again straight lines. They are drawn as dashed lines, for delays of 0.5, 1, 1.5, 2, 2.5, and 3 msec.

The highest order of F region reflection which can be propagated is limited by the F region critical frequency; the relevant frequency for each angle for an F region height of 250 km is inserted opposite the F axis on figure 4.

Since the nature of Es ionization is to occur in relatively intense patches, it will be assumed that the E mode is determined by its spatial extent, rather than its critical frequency as such. From eq (3), E propagation occurs for m/N_E of the path; if it is assumed that there must be on an average this amount of Es to support the mE nF mode of propagation, lines of constant fractional coverage of Es can be inserted on figure 4; they are shown for fractions of 0.2, 0.4, 0.6, and 0.8.

As an example, one may take an F critical frequency of 6 Mc/s and a fractional coverage of 0.2. All the points in the quadrilateral $ABCD$ will be possible orders of reflection; they are

$$3F,\ 4F,\ 5F$$
$$1E\ 3F,\ 1E\ 4F,\ 1E\ 5F$$
$$\bar{1}E\ 4F,\ \bar{1}E\ 5F,\ \bar{1}E\ 6F$$
$$\bar{2}E\ 6F.$$

The delays of these various orders can be interpolated between the straight lines of constant delay.

It is evident that when Es propagation becomes important each order of F reflection will have a series of E multiples associated with it, one set arriving earlier, the other set later, at the receiver. The interval between these successive orders of E reflection varies from 0.15 msec for the $3F$ reflection to 0.3 msec for the $7F$ reflection. If the Es ionization is present over a large proportion of the path, the E multiples associated with successive orders of F reflection overlap, giving a complex pattern.

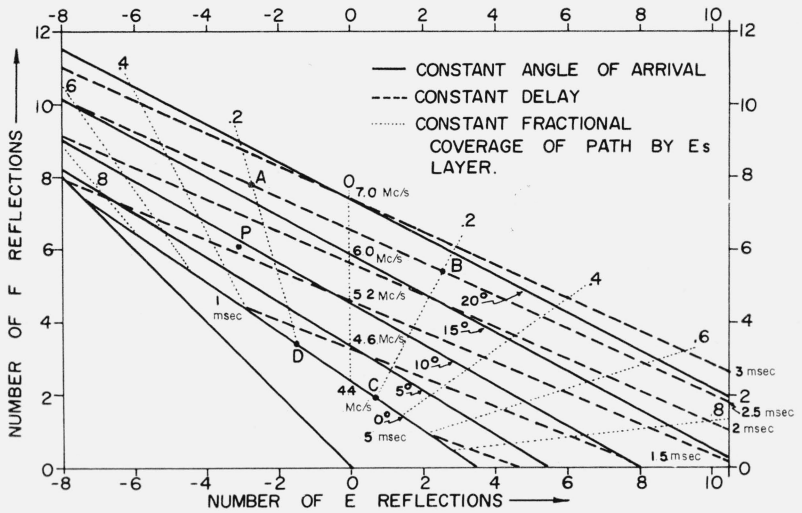

FIGURE 4. *Statistical effect of* Es *coverage.*

2.3. Extension to Thick Layer

Assuming the Breit and Tuve theorem to hold, the finite thickness of the reflecting layer may be allowed for by plotting the $h'f$ curve on figure 3, using the limiting frequency scale derived previously. The curve ABC on figure 3 represents the $h'f$ curve of a parabolic region, with the height of maximum ionization, h_m=300 km, semithickness 120 km, and critical frequency 7 Mc/s. The delays and angles of arrivals of the various orders of reflection which would be observed, if this layer were present throughout the path, are given by the intersections of this curve with the n=3, 4 etc., lines. In the limit of a very thin region, the curve ABC becomes a vertical line, terminating sharply at the critical frequency.

It should be noted that the curve ABC, if extended beyond the right edge of figure 3, will intersect the n=4 line again, at a higher angle of arrival. This, of course, represents the so-called "high ray" sometimes observed on oblique incidence paths.

3. Experimental Measurements

3.1. General Description

The experiments to be described used transmissions from an Air Ministry sender at Colombo, Ceylon, on a frequency of 16.16 Mc/s. The duration of each transmitted pulse was 100 μsec and a rhombic transmitting aerial was used, the polar diagram of which (see fig. 5) had a maximum at about 10° to the horizontal. The experiments commenced on the pulse transmissions at Baddow in April 1953, and continued until the end of January 1954. Apart from unavoidable breaks in transmission, the signals were sent out during daylight hours on one day every week. At the end of January 1954, some special transmissions were arranged by the Radio Research Board on four consecutive days. The cooperation of the Radio Research Board and the Air Ministry throughout the experiments proved most valuable.

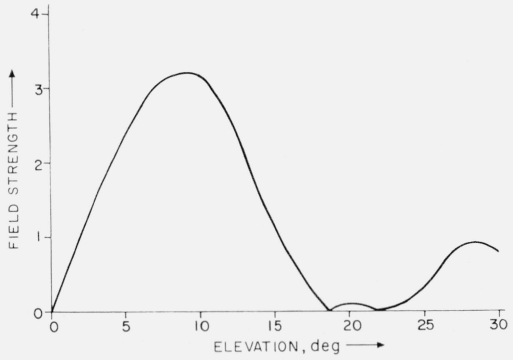

FIGURE 5. *Transmitting antenna polar diagram.*

3.2. Receiving Arrangements

The signal pulses were transmitted at a rate of 25/sec; by the time they reached the receiver, the presence of different propagation modes had lengthened them to about 1 msec. Consequently, some form of triggered time-base was necessary to display the incoming waveforms on a cathode-ray tube screen. Various methods using the signal itself to trigger the time-base proved unsuccessful since the signal frequently faded below local and atmospheric noise. As the source of 25 c/s at the transmitter was a highly stable crystal oscillator, a similar oscillator was later used at the receiving station.

The block diagram of the receiving equipment is shown in figure 6. The signals were received on a half-wave dipole antenna by a CR150 communication receiver, working on its widest bandwidth of 13 kc/s. Under some circumstances it was necessary to use a bandwidth of only 8 kc/s, due to the presence of powerful CW stations on nearby frequencies; however the difference in the observed pulse waveforms when these two bandwidths were used alternately, suggested that little information was lost by using the 8 kc/s bandwidth. The receiver output was displayed on an oscilloscope; the 25 c/s triggering impulses for the oscilloscope time base were derived

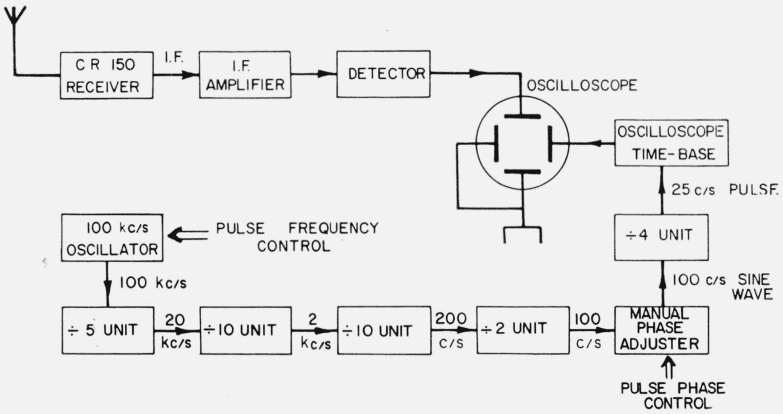

FIGURE 6. *Equipment block schematic.*

from a 100 kc/s crystal oscillator, the frequency of which could be altered by about 1 part in 4,000 by means of a frequency pulling circuit.

Two typical waveforms (instantaneous still photographs of the cathode ray tube display) are shown in figures 7(a) and 7(b). These photographs are two of the series described in section 5.2. It is seen that the length of the pulse train is over 1 msec, and that it may be quite complex.

3.3. Types of Echo Observed

To study the structure of the echo in detail, a method of recording was used in which the incoming signal voltage modulated the brightness of the oscilloscope trace. A photographic film, moved at right angles to the trace, then gave a record similar to the group-height-time records familiar in vertical incidence work.

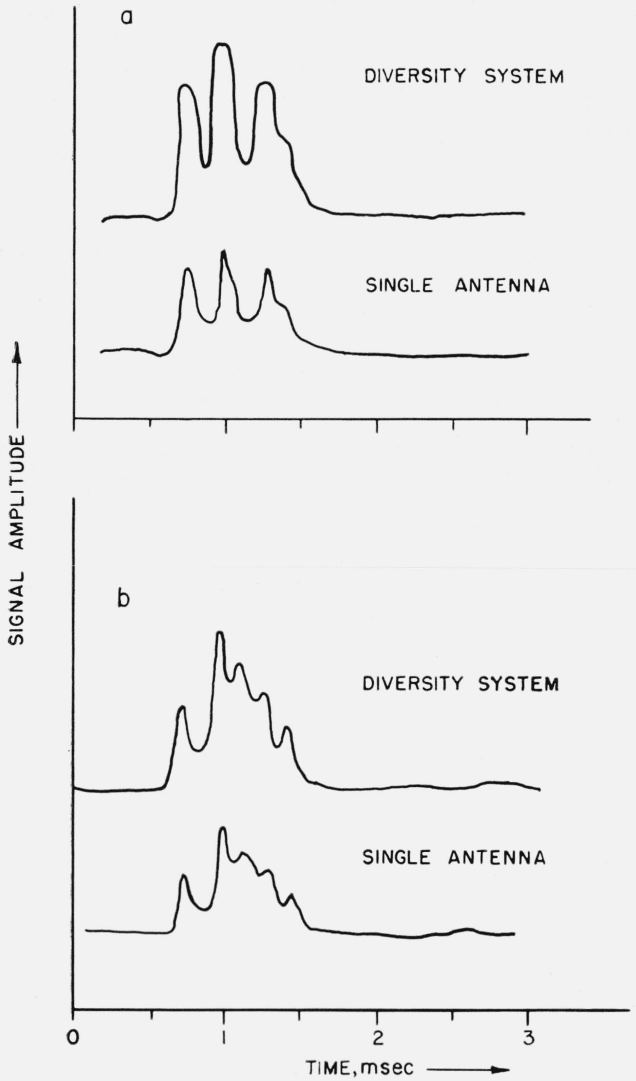

FIGURE 7. *Instantaneous pulse waveforms.*

Using this method of recording, the only attention the apparatus required was occasional adjustment of the crystal frequency, to ensure that the pulse pattern was kept about in the center of the oscilloscope time base.

Generally speaking, the signal was usually detectable from 1000 to about 1530 G.m.t.; on some occasions, the transmissions did not extend over the full period. The signal was usually at its strongest at about 1300 G.m.t., but no detailed measurements of signal strength were made. The type of pattern observed varied considerably with propagation conditions.

Figure 8 shows a simple type of pattern, in which the time base was applied vertically, with delay increasing upward. The sinusoidal variation in delay, with a period of about 10 sec, is due to imperfect synchronization of the pulse. The vertical white dashes are due to pulses of static, of very short duration; the striations in the trace near the left-hand edge are the result of CW interference from a transmitter on an adjacent channel.

In the summer, much stronger echoes are received on days when *Es* ionization is present. As shown in section 2.2, its effect is to generate a group of closely spaced echoes, centered on each order of *F* reflection. Depending on the geometry of reflection, the spacing may be from 0.1 to 0.2 msec. Figure 9(a) is an example of predominantly *Es* propagation, with only one order of *F* reflection present. The four components of the pulse have a mean separation of about 0.15 msec. Figure 9(b) shows an intermediate case, where four *F* echoes are present, with a small amount of *Es* causing each to split into three distinct echoes. In figure 9(c) the *Es* echoes have completely obscured the *F* echo pattern.

4. Comparison With Simple Ray Model

Designating the three pulses in figure 7(a) as *P*, *Q*, and *R*, in order of arrival, the time separation between pulses *P* and *Q* is about 0.24 msec, and between *Q* and *R* is about 0.28 msec. To explain these separations by a constant reflection height would lead to a height of only 200 km, from figure 2: this is clearly incompatible with the ionospheric data of section 2.1.

One possibility for explaining the various modes is in terms of low- and high-angle rays. The curve *GHI* on figure 3 represents a parabolic layer with height of maximum ionization 300 km, semithickness 120 km, and critical frequency 6 Mc/s. The points *G*, *H*, and *I* correspond to low and high angle third order *F* reflections, and a high angle second order reflection, respectively. This configuration produces a set of three modes with very nearly the observed overall separation: however, the two modes *H* and *I* occur with nearly identical delay, rather than the observed .28 msec separation. A departure of the layer from a parabolic form, giving a flattening of the "nose" of the layer, might displace point *I* to *J*, thereby removing the degeneracy. The ray would

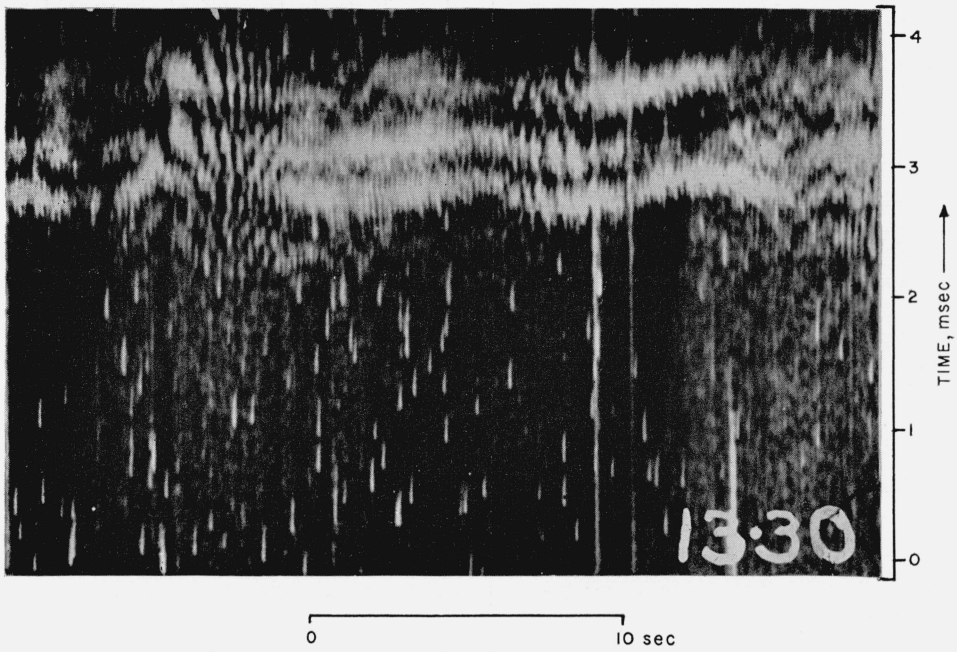

FIGURE 8. *Typical simple pattern.*

then arrive at a very low angle to the horizontal. On the whole, a flattening involving an equivalent vertical incidence group retardation of over 70 km for a frequency increment of less than 0.2 Mc/s seems unlikely, and Kift (1960) has suggested that high-angle modes propagated over great distances are unstable. However, this interpretation cannot be ruled out, particularly in view of the approximations involved in assuming uniform propagation characteristics over the entire path.

An alternative interpretation is that two of the three successive pulses of figure 7(a) have the same order of reflection but are different magneto-ionic components. On a thin-layer hypothesis (fig. 2), if pulses P and R are assumed to be the same component for the third and fourth order reflections, the delay between the two, 0.52 msec, corresponds to a reflection height of about 300 km, and their angles of arrival are about 5° and 11° respectively. If pulse Q is assumed to be a third order reflection, its effective reflection height must be about 335 km in order to account for the additional delay, and its angle of arrival must be about 7°. This might well be accounted for by pulses P and Q being the ordinary and extraordinary third order reflections respectively. Assuming the same parabolic layer as previously, the ordinary and extraordinary ray reflection conditions have been plotted on figure 3 as ABC and DEF respectively. It is suggested that the pulses P, Q, and R may correspond to the points A, D, and B respectively.

Since there appears to be some doubt as to which of these interpretations is correct, the pulses will be referred to by the letters P, Q, and R in subsequent sections.

5. Fading Analysis

Using the analysis of the previous sections as a basis, the principal characteristics of the fading observed over this path will now be described.

5.1. Simple Echo Fading

On a limited number of occasions, only a single order of reflection was present in the pattern. At these times, an easily interpretable fading curve could be obtained by photographic recording; an example is shown in figure 10. The upper and lower traces are the fading curves received at two antennas of a space diversity pair, 600 ft apart in a line perpendicular to the direction of propagation. There is clearly a high correlation between these curves, indicating a distance scale of much greater than 600 ft in the random diffraction pattern.

5.2. Complex Echo Fading

When only a single order of reflection is present, the fading of a pulsed signal is identical with that of a CW signal, and only fluctuations in amplitude are important. If a CW signal is composed of several orders of reflection, however, the possibility of phase interference between the various echoes may give both a faster rate of fading and a smaller structure size on the ground (greater diversity in a space-diversity system).

This comparison may be readily effected by switching the receiving system bandwidth. If a wide bandwidth is used in the receiving system, so that the orders of reflection are resolved, each order will de-

scribe its own fading curve. However, if the bandwidth is narrowed to such an extent that the pulses completely run into one another, thus approximating to the CW case, then the resultant fading will be due not only to the fading of the orders of reflection, but to the effect of phase interference between them.

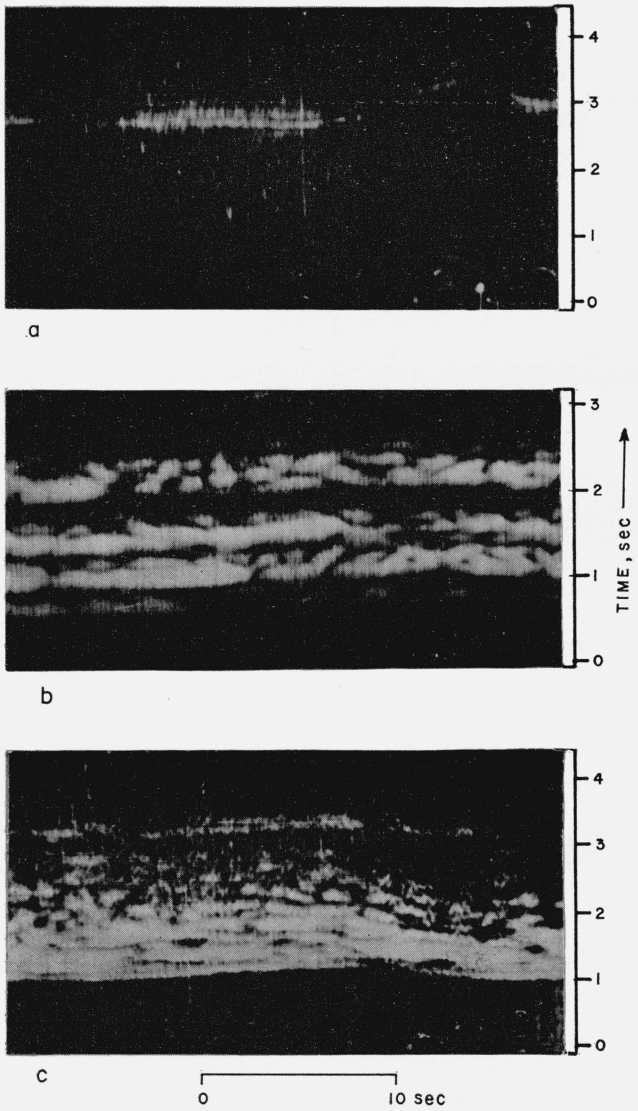

FIGURE 9. *Pattern showing* Es *echoes.*

To illustrate this effect, figure 11 shows four successive stretches of fading record, in which the receiver bandwidth was switched from 8 kc/s to 1 kc/s instantaneously. There is complete diversity between the two 1 kc/s signals in 11*B* and 11*D*, but the 8 kc/s signals of 11*A* and 11*C* display marked correlation. In order to study the rapid fading of the various elements of the pulse waveform in detail, and to relate this to the behaviour of a diversity receiving system, photographs were taken of the pulse waveform at 2-sec intervals. Two examples of these photographs were shown in figure 7. In each case the upper waveform represents the pulse received by a four-fold diversity system, i.e., the mean of four-pulse patterns received on four separate antennas and receivers. The other pulse shown was that received simultaneously on a single antenna.

To remove the possibility of slight random jitter of the pattern, the average of a number of waveforms was first calculated, and is shown in figure 12. With this as a guide, the individual waveforms were synchronized, and peak values read off for the *P*, *Q*, and *R* reflections. The mean values of these quantities are shown with circles on figure 12. They are greater in amplitude than the previously measured peaks of the three pulses, due to slight lack of synchronism in calculating figure 12.

Typical fading curves for the various pulses for a single antenna and for a diversity system are shown in figures 13, 14, and 15.

5.3. Diversity Comparison

Several interesting points are immediately evident from figures 11, 12, and 13. Firstly the depth of fading for the three pulses is quite different, being much less for the *Q* reflection than for either the *P* or the *R*. The best measure of this depth of fading is the ratio of the standard deviation of the fading curve to its mean value. If the depth of fading is defined as *D*, then

$$D=\frac{\sqrt{\overline{x^2}-\overline{x}^2}}{\overline{x}}$$

where x=amplitude of fading curve at any instant. Values of *D* are given in table 2 for the three pulses. For a single aerial, the values of *D* are 0.35 and 0.34

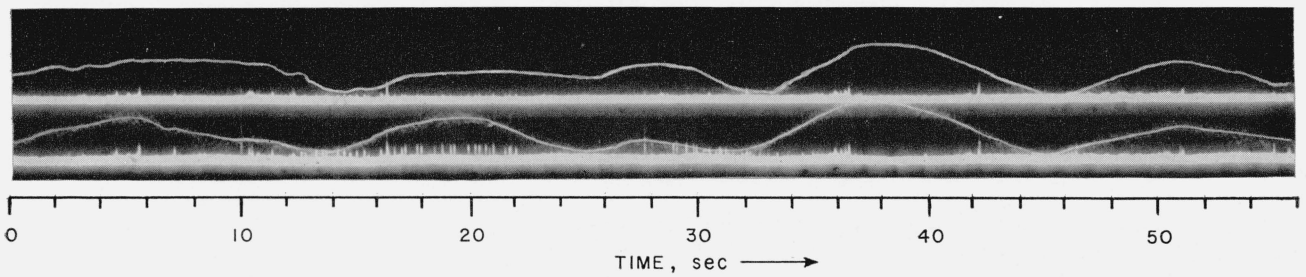

FIGURE 10. *Spaced antenna fading curves—single echo.*

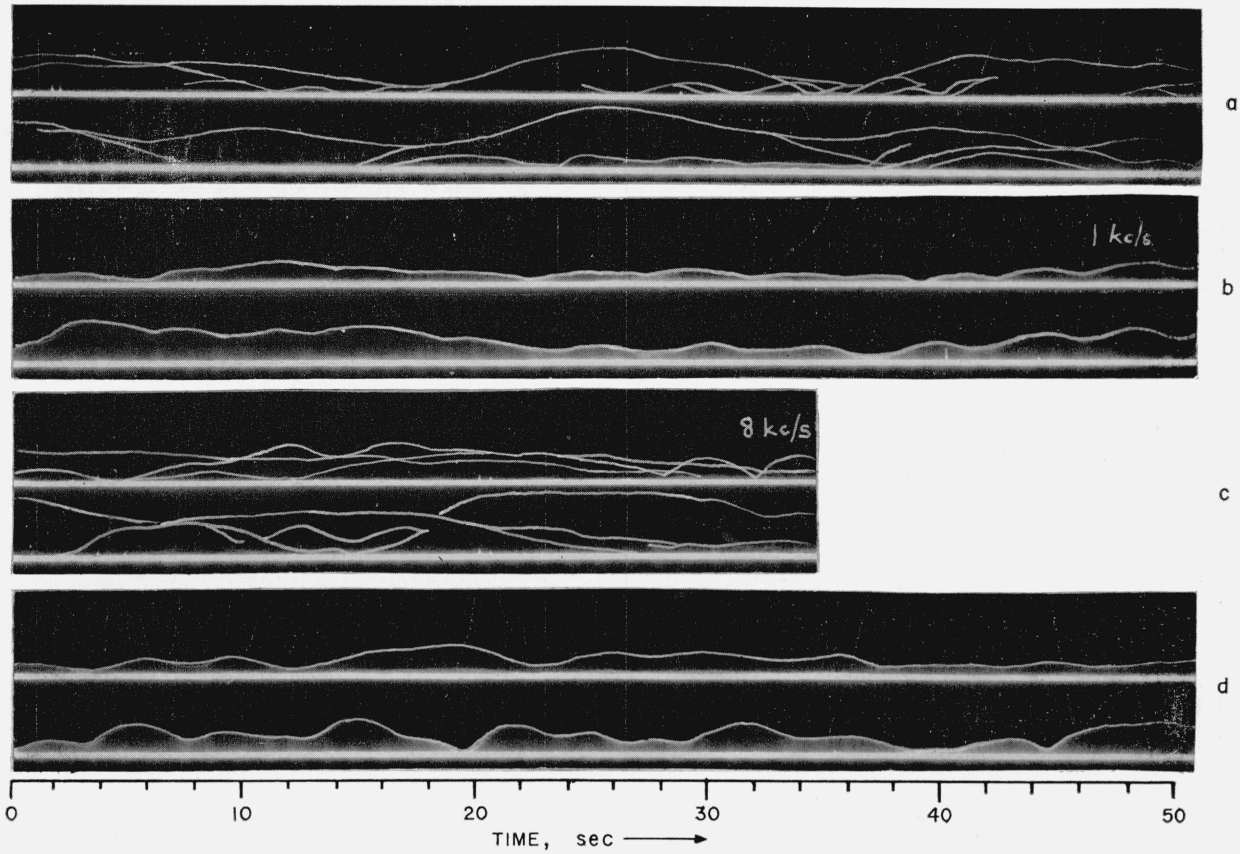

FIGURE 11. *Spaced antenna fading curves—multiple echoes.*

TABLE 2

Pulse	Aerial	Mean signal	D	ρ_1	U
					sec
P	Single	12.7	0.353	0.439	3.0
	Diversity	19.1	.367	.466	2.9
Q	Single	29.1	.174	.450	2.5
	Diversity	43.5	.173	.465	2.9
R	Single	15.5	.343	.343	2.1
	Diversity	24.5	.306	.065	1.5

for the P and R pulses, but only 0.17 for the Q pulse. The greatest value of D which would be expected experimentally would be the value for a signal with a Rayleigh probability distribution, which would give a value of 0.52.

Though the diversity system has virtually no effect on the depth of fading for two of the echoes received, this does not mean that it would also be ineffective for a CW signal; since in CW reception the different orders of reflection may interfere destructively. The only condition for a diversity system to give an improvement in the communication system performance is that the phase relation between the echoes shall be different at the four diversity antennas.

The difference in fading speed of the three pulses should be noted. The fading periods of the P and Q pulses are about 1 cycle in 5 to 10 sec. The fading of the R pulses, however, is very much more rapid. The best quantitative measure of the fading speed is the correlation function of the amplitude. The first ordinate of this is the correlation ρ_1 between the amplitudes of the same pulse in successive snapshots (taken at 2-sec intervals). These correlation coefficients are given in table 2. If it is assumed that the time correlogram of the fading curves has a Gaussian form, i.e.,

$$\rho(\tau)=e^{-6.58\tau^2/U^2}$$

where $\rho(\tau)$ = correlation between amplitudes separated by a time interval τ,

U = average time between peaks of fading curve,

= "fading period" of curve,

then the fading period of the pulse amplitudes can be calculated. These values of U are also given in table 2.

Another feature of the fading curves is the effect of the diversity system on the fading of the various

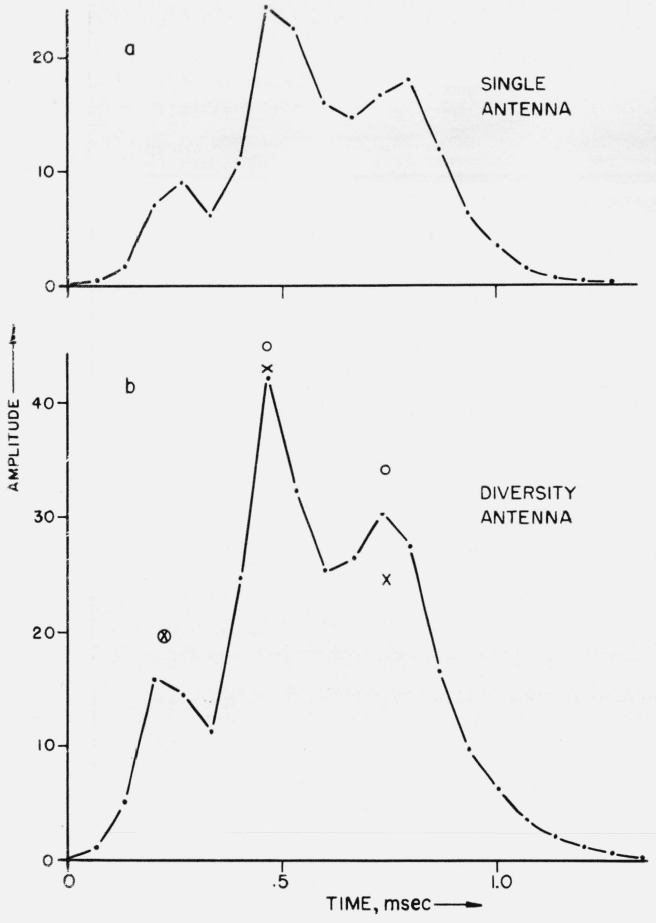

FIGURE 12. *Average pulse waveforms.*

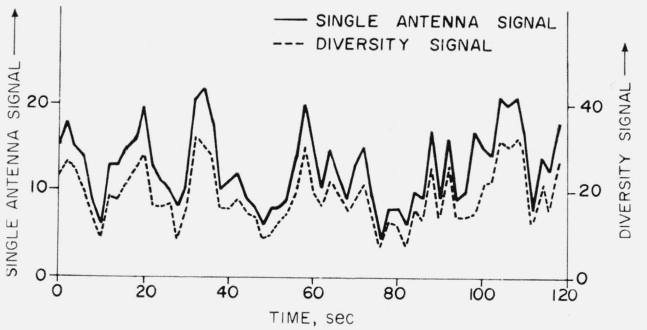

FIGURE 13. P *pulse amplitude.*

pulses. If the amplitudes of the pulses at the four antennas were completely unrelated, then the value of D for the diversity combination of these four should only be half that for the pulses received on a single antenna. In fact, however, as can be seen from table 2, the value of D for the P and Q reflections is nearly the same whether a single aerial or a diversity system is used, indicating that for these pulses the amplitudes received at the diversity antenna were practically identical. Only in the case of the rapidly fading pulse, P, is there an appreciable difference in the values of D.

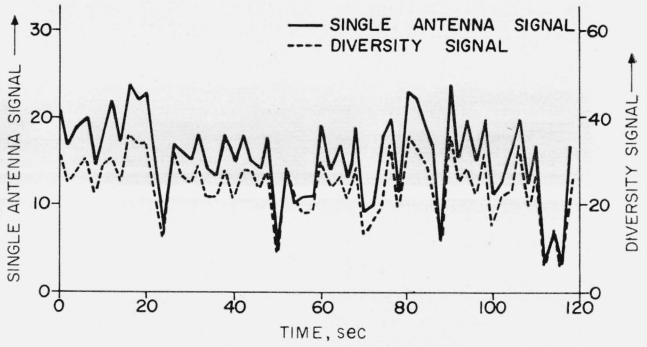

FIGURE 14. Q *pulse amplitude.*

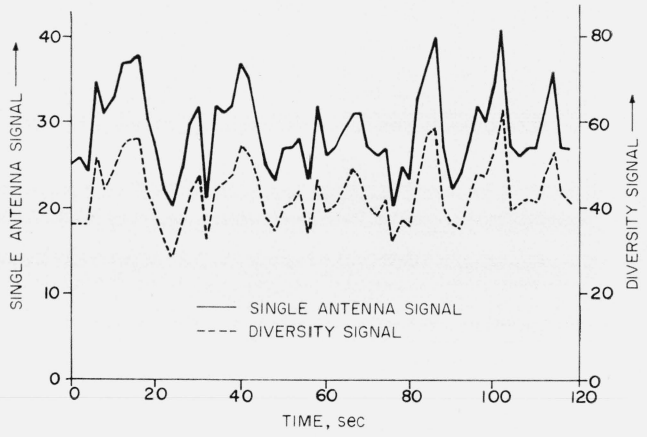

FIGURE 15. R *pulse amplitude.*

A simple relation is derived in the appendix between the depth of fading from a diversity system and the original depth of fading of the single aerial signal, in terms of the average correlation between the signal amplitudes received by the various diversity aerials. The simple theory also correctly predicts the correlation between the single antenna amplitude and the diversity amplitude.

6. Conclusion

The work which has been described was originally intended to clarify the meaning of measurements of diversity at high frequencies. The fading of the different modes of propagation were studied separately, and it was shown that the diversity arose both through diversity of the modes of propagation themselves, and also through phase interference between them; which of these is the major source of diversity depends on the degree of complexity of the pulse pattern.

The need to identify the pulses received led to a consideration of the way in which a steady signal was propagated over long distances; it has been shown that the "sky billiards" approach of geometrical optics gives an adequate explanation of the experimental observations.

It is suggested that when the propagation is simple, i.e., when there is only one predominant order of reflection present, the deversity of a CW signal is due to the irregularities in the reflecting layer; but when the propagation is complex, with many orders of reflection present, the diversity of the CW signal is due principally to phase interference between the orders of reflection.

7. Appendix. Theory of n-Fold Diversity Combination

A diversity signal is formed by averaging n signals $R_1 R_2 \ldots R_n$ to give a signal R_D. It is required to find.

1. The ratio A by which the standard deviation σ of the original signals is reduced by the process of averaging.

2. The correlation of the average with any one of the signals. It will be assumed that the correlation of each signal with every other signal is equal to ρ.

1. $$n^2 \cdot \overline{R_D^2} = \overline{(R_1 + R_2 + \ldots + R_n)^2}$$

$$= n^2 \overline{R}^2 + n\sigma^2[1 + (n-1)\rho]$$

$$\therefore A = \sqrt{\frac{1 + (n-1)\rho}{n}}$$

$$\text{or } \rho = \frac{nA^2 - 1}{n-1}.$$

For the R pulse of section 5.3, $A = \frac{0.306}{0.343} = 0.892$

$$\text{or } \underline{\rho = 0.73}.$$

2. $$\overline{R\,R_D} = \frac{1}{n} \Sigma \overline{R\,R_D} = \overline{R}^2 + \sigma^2[\rho + (1-\rho)/n]$$

$\therefore$ Correlation between R and R_D

$$= \frac{\sigma^2[\rho + (1-\rho)/n]}{\sqrt{\sigma^2 \cdot \sigma^2[\rho + (1-\rho)/n]}} = A.$$

So, taking the previous example,

correlation between R and $R_D = 0.89$

This compares with the value of 0.887 calculated directly from the observations of section 5.3, indicating the accuracy of this theory.

8. References

Kift, F., The propagation of high-frequency radio waves to long distances, Proc. IEE **107** pt. B, 127–140 (March 1960).

Silberstein, R., A long-distance pulse-propagation experiment on 20.1 megacycles, J. Geophys. Research **63,** 445–466 (Sept. 1958).

Wilkins, A. F., and F. Kift, Characteristics of H.F. signals, Electronic and Radio Engineer **34,** 335–341 (Sept. 1957).

(Paper 65D3–121)